A simple model for the wall depletion length of nanoconfined DNA

Aditya Bikram Bhandari,[1] Jeffrey G. Reifenberger,[2] Hui-Min Chuang,[1] Han Cao,[2] and Kevin D. Dorfman[1, a)]

[1)] *Department of Chemical Engineering and Materials Science, University of Minnesota – Twin Cities, 421 Washington Ave SE, Minneapolis, MN 55455, USA*

[2)] *BioNano Genomics Inc., 9640 Towne Centre Drive, Suite 100, San Diego, CA 92121, USA*

(Dated: 17 May 2018)

We have measured the wall depletion length of DNA confined in 38 nm wide, square silicon dioxide nanochannels for five different ionic strengths between 15 mM and 75 mM. Experiments used the BioNano Genomics Irys platform for massively parallel data acquisition, attenuating the effect of the sequence-dependent persistence length and finite-length effects by using nick-labeled *E. coli* genomic DNA with contour length separations of at least 30 μm (88,325 base pairs) between nick pairs. In excess of 5 million measurements of the fractional extension were obtained from 39,291 labeled DNA molecules. Analyzing the stretching via Odijk's theory for a strongly confined wormlike chain yielded a linear relationship between the depletion length and the Debye length that is in qualitative agreement with previously defined analytical models.

[a)] Electronic mail: dorfman@umn.edu

I. INTRODUCTION

The past decade has witnessed a sustained effort to develop a theory for the properties of a semiflexible polymer confined to a nanochannel, inspired by the seminal experiments by Reisner *et al.*[1] on channel-confined DNA that suggested that the classical theories by Daoud and de Gennes[2] and Odijk[3] were incomplete. There now exists a relatively complete theoretical framework describing the equilibrium properties of a confined semiflexible chain. At the scaling level, the four-regime theory by Odijk[4] has been confirmed by various simulations.[5–11] Indeed, in the asymptotic limits embodied by his scaling theory, the prefactors are now known to high precision for both very strong confinement[12,13] and the marginal solution case[8] typically referred to as the extended de Gennes regime.[14] For cases where the asymptotic limits of the theory are not satisfied, which is often the case in practice, the recently-proposed correlated telegraph model provides quantitative agreement with simulations for situations where the configuration is dominated by hairpin formation rather than alignment fluctuations,[15] reproducing two of Odijk's regimes as limiting cases. While theory and simulation are now in accord, attempts to test these theories using DNA as a model polymer[1,16–22] have been stymied by a poor understanding of the depletion length characterizing the reduction in cross-sectional area of the channel available to the DNA due to DNA-wall interactions. In the present contribution, we combined a massively parallel experimental system based on genome mapping[23] with the exact result for the fractional extension in the Odijk regime[13] to measure the depletion length between DNA and a silica nanochannel.

DNA has many attractive properties as a model system for testing the theory of channel-confined polymers. Most importantly, the DNA contour length is computed easily, the confined polymer is visualized readily by fluorescence microscopy, and the persistence length of DNA is commensurate with the length scales that are accessed by nanofabrication techniques. However, the polyelectrolyte nature of DNA complicates the comparison of experimental data obtained in a nanochannel with theory, as the most pertinent theories[4,14,15] are derived for a neutral polymer. This problem can be attenuated to some extent by working at high ionic strengths, in the 10-100 mM range, where the electrostatic screening length is small compared to the other length scales in the problem. The theories for the persistence length[24] and effective width[25] of a polyelectrolyte are mature, and their dependence on ionic

strength at such high ionic strengths is relatively weak.[26] Moreover, at high ionic strengths, the Kuhn segments have an aspect ratio of approximately 20,[26] which is sufficient to test some but not all aspects of the prevailing theories.[9]

However, to compare theory to an experiment performed in a channel size D, is it imperative to know the value of the effective channel size

$$D_{\text{eff}} = D - \delta \tag{1}$$

that is available to the polymer. In the latter, δ is the depletion length characterizing the region of the channel that is inaccessible to the DNA due to the combination of excluded volume and electrostatic interactions. Many studies approximate the depletion length as being equal to the effective width w of the DNA; i.e., the DNA-wall interactions are modeled by the same hard-core potential as the intersegmental DNA interactions after the latter have been mapped from those for a polyelectrolyte to an equivalent neutral chain.[25] This ubiquitous approximation finds its justification in early work comparing simulations to experiments,[5] where adjusting the actual channel size by the effective width of the DNA provided improved agreement. A subsequent study[19] using $\delta = w$ typically yielded 10% error between simulation and experiment. While this level of agreement is satisfactory from an engineering perspective, it is insufficient to draw conclusions about the validity of theories for confined DNA, in particular when the theoretical prefactors are known to high precision.[14,18,20,22] Indeed, the uncertainty in δ has been cited multiple times as a possible source of systematic error.[18,20,27]

In this contribution, we present data for the DNA extension as a function of ionic strength obtained using the BioNano Genomics Irys platform. This is a massively parallel system for obtaining experimental data at the single molecule level, allowing us to make over 5 million measurements of fractional extension using images of 39,291 individual, nick-labeled DNA molecules by measuring the extension between widely spaced nick pairs along these molecules. Our current study follows a line of recent work[21,28–32] where this genome mapping platform has been used to studying fundamental physical problems with unprecedented data density, albeit only over the narrow range of channel sizes where genome mapping can extract the contour length of the randomly sheared genomic DNA injected into the device. Here, we leverage the exact result for the Odijk regime[13] to compute the effective channel size for the DNA as a function of ionic strength in 38 nm wide, square nanochannels, which in turn furnishes the depletion length by Eq. (1). These measurements allow us to analyze existing

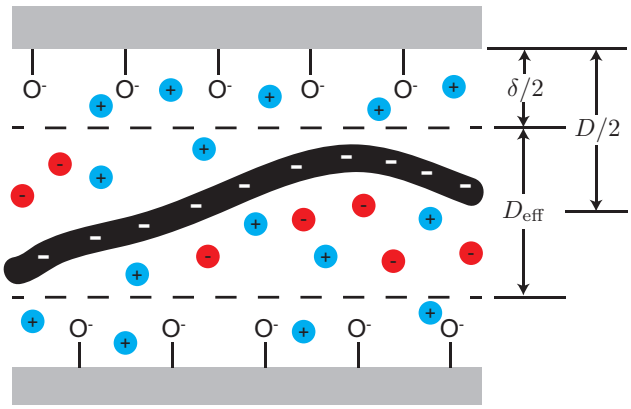

FIG. 1. A DNA molecule confined in an electrolyte-filled nanochannel. Both the DNA molecule and the surface of the nanochannel are negatively charged. The difference between the effective channel size D_{eff} available to the DNA molecule and the actual channel size D is the depletion length δ.

models for the depletion length[5,27] as well as re-evaluate the agreement between an exact result for the fractional extension of confined DNA in the extended de Gennes regime[14] and previous experimental studies.[18,20,22] The key outcome of our analysis is a simple model for the depletion length of DNA in a high ionic strength buffer, which we envision will prove useful in future attempts to use DNA as a model system for confined polymers.

II. THEORY

Figure 1 provides a schematic illustration of the depletion length for a DNA molecule confined in a silicon dioxide nanochannel of width D. The hydration of the silicon dioxide surface network by water[33] to form silicon hydroxide followed by its subsequent deprotonation[34] at pH greater than 7 leads to the formation of SiO^- groups and hence a negative charge at the channel surface.[35] Owing to the electrostatic interactions between the negatively charged DNA and the wall, there is a depletion length $\delta/2$ near the wall where the DNA is effectively excluded; the sum of the depletion lengths from the upper and lower walls of Fig. 1 is the total depletion length δ. The magnitude of the depletion length is affected by the electrostatic screening provided by the excess salt in the buffer. Hence, the depletion length should be a function of, at least, the linear charge density of the DNA, the surface charge density of the walls, and the ionic strength of the solution.

There are three models for the depletion length. The most commonly used approximation for δ is to consider it equal to the effective width, w, that characterizes the DNA-DNA excluded volume interactions,

$$\delta = w \tag{2}$$

By mapping the osmotic pressure of two charged cylinders of linear charge density ν_{eff} to that of two neutral cylinders of width w, Stigter[25] showed that the effective width of DNA is given by

$$w = \lambda_{\text{D}} \left[0.7704 + \log \left(\frac{\nu_{\text{eff}}^2 \lambda_{\text{D}}}{2\epsilon\epsilon_0 k_{\text{B}} T} \right) \right] \tag{3}$$

where

$$\lambda_{\text{D}} = \left(\frac{\epsilon\epsilon_0 k_{\text{B}} T}{2 N_{\text{A}} e^2 I} \right)^{1/2} \tag{4}$$

is the Debye length, ϵ is the dielectric constant of the medium, ϵ_0 is the permittivity of free space, $k_{\text{B}}T$ is the product of the Boltzmann constant and the absolute temperature, N_{A} is Avagadro's number, e is the elementary charge, and I is the ionic strength of the buffer. The effective linear charge density ν_{eff} appearing in Eq. (3) has a complicated dependence on the ionic strength I of the solution, as it is computed by determining the linear charge density ν_{eff} in a Debye-Hückel model of the surface charge that, in the far field, provides the same potential as that produced by the nonlinear Guoy-Chapman model with the true charge density of the DNA.[36] Clearly, the excluded volume produced by two charged rods of the same linear charge density should not be the same as that produced between a charged rod and a surface of differing chemistry. Nevertheless, the approximation $\delta = w$ has found widespread use since Wang *et al.*[5] showed that it provides reasonable agreement between experimental and simulation data obtained at different ionic strengths.

The second model for the depletion length is attributed to Derek Stein.[27] In this model, the charged surface produces an electric potential

$$\psi(z) = \frac{4k_{\text{B}}T}{e} \tanh \left(\frac{e\zeta}{4k_{\text{B}}T} \right) e^{-\kappa z} \equiv \psi_{\text{wall}} e^{-\kappa z} \tag{5}$$

In the latter, ζ is the zeta potential of the wall, $\kappa = \lambda_{\text{D}}^{-1}$ is the inverse of the Debye length, and z is the distance away from the surface. The DNA is envisioned as a charged, semiflexible polymer interacting with the electric potential ψ created by the wall. By assuming that only those segments within a distance λ_{D} of the segment closest to the wall contribute to

the DNA-wall electrostatic interaction, the resulting depletion length is :

$$\delta = 2\lambda_{\mathrm{D}}\left[0.5772 + \log\left(\frac{\sqrt{\pi}\nu_{\mathrm{eff}}\psi_{\mathrm{wall}}(l_{\mathrm{p}}\lambda_{\mathrm{D}}^2)^{1/3}}{k_{\mathrm{B}}T}\right)\right] \tag{6}$$

where l_{p} is the DNA persistence length.

The last model was proposed by Reisner *et al.*,[27] who considered the DNA as a charged, rigid rod with hindered rotation due to the wall, rather than a semiflexible chain. The resulting depletion length for this model is

$$\delta = \lambda_{\mathrm{D}}\left[1.5772 + \log\left(\frac{\nu_{\mathrm{eff}}\psi_{\mathrm{wall}}\lambda_{\mathrm{D}}}{k_{\mathrm{B}}T}\right)\right] \tag{7}$$

Owing to their similar origins, the models in Eqs. (2), (6) and (7) all have a similar functional form,

$$\delta = c_1\lambda_{\mathrm{D}}\left[c_2 + \log(F)\right] \tag{8}$$

where F is a function of ionic strength embodied by ν_{eff}, ψ_{wall} and λ_{D}, that captures the microscopic details of the excluded volume interactions.

For a given value of the ionic strength, the Deybe length is given by Eq. (4) with $\epsilon = 80$ for water, the DNA persistence length can be obtained using Dobrynin's theory,[24]

$$l_{\mathrm{p}}[\mathrm{nm}] = 46.1 + \frac{1.9195}{\sqrt{I[\mathrm{M}]}} \tag{9}$$

and the effective charge density is computed from Stigter's theory.[36] The wall potential, ψ_{wall}, is calculated using Eq. (5) from Behren and Grier's model[37] for the zeta potential ζ. Briefly, we compute ζ by simultaneously solving the equation set

$$\zeta(\sigma) = \frac{k_{\mathrm{B}}T}{e}\log\left(\frac{-\sigma}{e\Gamma + \sigma}\right) - (p\mathrm{H} - p\mathrm{K})\frac{k_{\mathrm{B}}T\log(10)}{e} - \frac{\sigma}{C} \tag{10}$$

and

$$\sigma(\zeta) = \frac{2\epsilon\epsilon_0 k_{\mathrm{B}}T}{e\lambda_{\mathrm{D}}}\sinh\left(\frac{e\zeta}{2k_{\mathrm{B}}T}\right) \tag{11}$$

where σ is the surface charge density, $\Gamma = 8$ nm^{-2}, $p\mathrm{K} = 7.5$, and $C = 2.9$ F/m^2 are the chargeable site density,[38] dissociation constant,[39] and Stern layer capacity[39] for silicon and glass surfaces. Our experiments use the BioNano Flow Buffer, which has a $p\mathrm{H}$ of approximately 8.6. Using the ζ-potentials for this buffer and Eq. (5), the resulting ψ_{wall} ranges from 99 meV to 101 meV for the ionic strengths of interest; for subsequent analysis, we simply used $\psi_{\mathrm{wall}} = 100$ meV.

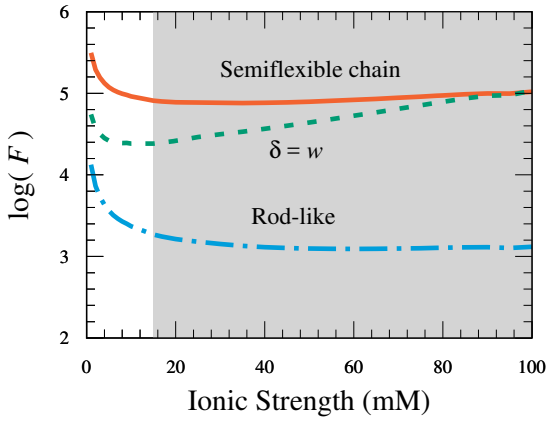

FIG. 2. The logarithmic terms in Eq. (2) (dashed green line), Eq. (6) (solid orange line) and Eq. (7) (dot-dashed blue line) versus ionic strength. The shaded region indicates the ionic strengths used in our experiments.

Figure 2 shows how the function F depends on ionic strength for DNA and a silica wall for each of the models. The shaded region indicates the ionic strengths used in our experiments. This range encompasses the ionic strengths used in a number of previous studies[1,16,18,21,40–43] that form an important database for comparing DNA confinement experiments to theories developed for a neutral polymer.[15] While F in the expression for effective width in Eq. (3) increases by about 15% as ionic strength increases, the values of F for the rod-like model and the semiflexible chain model are fairly constant for the higher ionic strengths of interest here, only starting to vary at very low ionic strengths. Using these constant regions of Fig. 2, the semiflexible chain model of Eq. (6) predicts $\delta \approx 11.05\lambda_D$ while the rod-like model of Eq. (7) predicts $\delta \approx 4.73\lambda_D$ and the $\delta = w$ model of Eq. (2) does not predict a linear relationship. As a result, we expect that the depletion length for the first two models will be proportional to the Debye length, with the details of the polymer-wall interactions (rod-like versus semiflexible chain) only appearing in the proportionality constant.

III. EXPERIMENTAL METHODS

E. coli genomic DNA (4,639,675 base pairs (bp)) was extracted from MG1655 cells as previously described.[29] The extracted DNA was nick-labeled at Nt.BspQI recognition sites (GCTCTTC) using the standard BioNano Genomics protocol[23,44,45] with a cy3-like fluores-

cent dye. The nicks were then repaired using *Taq* ligase and the backbone stained overnight using YOYO-1 at a dye to base pair ratio of 1:37. The DNA was suspended in the BioNano Flow Buffer with no NaCl (I = 16.88 mM, containing 10 wt% poly(vinyl pyrrolidone),[46,47] available from BioNano Genomics). All experiments were conducted at room temperature and pressure.

The DNA was loaded onto a BioNano Genomics Irys v2 Chip (8 μL solution added to both the inlet and the outlet) with approximately square channels of width 38 nm and length 1 mm, using a custom electrophoresis script.[46] We estimate the error in the channel size to be ±2.5 nm which propagates to an equivalent uncertainty in the measurement of δ. The DNA molecules, electrokinetically driven into the channels, were imaged using an Olympus IX-71 microscope with an Olympus 60x air objective (NA = 0.90) and an Andor Zyla 5.5 sCMOS camera. The nick sites with cy3-like fluorophore and the YOYO-stained backbone were excited using a Sapphire (532 nm, 300 mW, Coherent) and an OBIS (488 nm, 150 mW, Coherent) laser, respectively. The exposure time for the green laser was set at 100 ms and the blue laser at 50 ms. Six scans of 160 frames each were taken of the DNA in the nanochannel, alternating between green and blue excitation. Figure 3 shows a typical image from the experiment with the green and blue channels combined. Only those labels that can be definitively associated with a DNA molecule were used for subsequent analysis.

After each run, a pillar blast was performed by focusing the laser at the entrance of the channel at a very high exposure to remove any DNA stuck on the pillars, and the ionic strength of the flow buffer was incremented. In order to avoid systematic errors involved in using a different chip and DNA sample for each ionic strength, the ionic strength was increased by pipetting out 0.5 μL of DNA solution and adding an equal volume of an NaCl solution to the inlet and outlet of the same Irys chip in order to increase the NaCl concentration to 2.5, 5, 30 and, finally, 60 mM. As this method involves incrementing the salt concentration by replacing $\approx 6\%$ of the buffer content in the chip with NaCl solution in water, we have adjusted the ionic strength of the preceding buffer contents to account for their dilution and considered the maximum error in the reported ionic strength as 10% of the ionic strength of the preceding buffer solution. We view this as a very conservative estimate of the error. After each salt addition step, the chip was conditioned using a potential of +2 V and -2 V, alternating every 200 s, for 4 cycles to ensure uniformity of buffer throughout the chip reservoirs and channels, and then the DNA were loaded into the channels. Typical

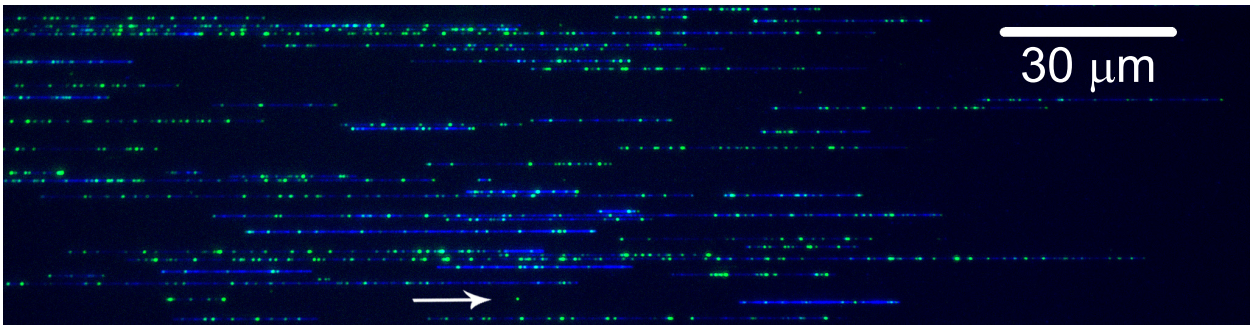

FIG. 3. False-color image of DNA in the nanochannels. The blue-colored backbone is labeled with YOYO-1 while the green dots within the backbone are the Nt.BspQI nick sites. An image processing algorithm further processes the image to select the molecules which correspond to a blue line and choose the nick sites based on a minimum intensity of the green channel. Green labels with a very low intensity blue backbone (arrow in the bottom left), indicative of molecules that have not been stained properly or free labels, are discarded by the algorithm. The scale bar is representative of the minimum allowed separation between any two nick pairs on the same molecule — nick pairs shorter than this length were not included for further analysis to avoid finite-length effects[6] and the sequence-dependent persistence length effect.[31]

TABLE I. Details of experimental conditions and calculated parameters

I (mM)	l_p (nm)	pH	ν_{eff} (e/nm)	λ_D (nm)	w (nm)
16.9	60.9	8.64	2.8	2.4	12.2
18.5	60.2	8.64	2.9	2.3	11.7
20.0	59.7	8.64	2.9	2.2	11.3
44.4	55.2	8.60	3.9	1.5	7.8
72.2	53.2	8.58	4.9	1.1	6.4

imaging times were 1.5 hr for each ionic strength.

For each of the solutions, the ionic strength (I), persistence length (l_p), solution pH, DNA effective line charge density (ν_{eff}), Debye length ($\lambda_D = \kappa^{-1}$) and DNA effective width (w) were calculated using a custom MATLAB script described elsewhere.[19] The results are listed in Table I.

The images obtained were processed using the psfDetect algorithm (available from Bio-Nano Genomics) and aligned to the *E. coli* MG1655 reference genome using the RefAligner

algorithm[48] at a genomic coverage in excess of 250-fold for each ionic strength and an alignment hit rate of approximately 61%. We posit that the relatively low degree of alignment is due to the inherent variability in the *E. coli* genome.[49–51] The result of the molecule alignment protocol is a file containing all of the molecules that are longer than 150 kbp and which aligned to the reference genome, along with the positions of their nick labels along the backbone and the corresponding nick sites on the reference.

The distance X between any two nick sites in the images was calculated using the conversions 366 bp = 1 pixel for the psfDetect algorithm and 1 pixel = 0.1083 μm for the microscope optics.[29] For the corresponding nick pairs in the reference genome, the contour length L was approximated as equal to the rise per base pair DNA, 1 bp = 0.34 nm. The very low dye loading used in our experiments should have a negligible effect on the contour length of DNA[1,19,52] and the mechanical properties of DNA.[31,53–55] The fractional extension for a given pair of labels is the ratio X/L.

All possible nick pairs from the 1,019 Nt.BspQI nick sites in the reference genome for *E. coli* MG1655 were tabulated and mapped to the individual nick sites on the molecules that aligned to the reference genome. Pairs separated by a distance less than 2,500 bp were disregarded as this genomic distance is close to the microscopy resolution limit.[31,56] This initial choice, which is a standard part of our image processing pipeline,[31] will ultimately prove inconsequential, as we will later restrict nick pairs to a minimum separation of 88,235 bp for reasons discussed in the next section. For each nick pair, we noted the number of molecules on which that particular pair was present, the contour length between the nick pair in the reference, the distance between the nick labels in the images, the average % GC content between the pairs, and the fractional extension. Only nick pairs with number of occurrences greater than 30 were chosen to keep in accordance with the central limit theorem for accurate statistical analysis. This operation removed ~ 90% of the total number of nick pairs, notably those separated by very long distances along the genome that could only be present in a data set containing large quantities of megabase pair DNA.

IV. RESULTS

The output of our experiment is an ensemble of fractional extensions, X/L, for each of the five ionic strengths in Table I. In analyzing these data, it is important to avoid two

sources of systematic error. First, for short distances between the nick labels, finite-size effects impede the use of Odijk's theory.[6] Second, the persistence length varies as a function of the % GC content between the nick sites.[31] We thus first undertook a systematic effort to remove these possible sources of error in our ensemble.

Finite-length effects appear as noise in the data set for the fractional extension, in particular as anomalously large values of X/L due to errors in the microscope resolution, anomalously small values of X/L due to folding of the chain ends, or misaligned molecules owing to the presence of false positive or false negative labels. For the Odijk regime, previous simulations[6] of DNA in a 30 nm channel suggest that finite-length effects can be safely ignored for chain lengths that exceed 100 persistence lengths. From the data in Table I, we expect to be in long-chain limit for contour lengths that exceed approximately 6 μm. The minimum considered distance between nick pairs was systematically increased in the course of our analysis from 2500 bp (approximately 0.85 μm), which is the resolution limit of the microscope, to 5 μm, 10 μm, 20 μm and finally 30 μm. We found that imposing the 30 μm cutoff on the minimum value of L helped (i) eliminate noise in the fractional extension distribution, (ii) narrow the GC content to minimize the effect of sequence dependent persistence length, and (iii) minimize the number of misaligned molecules due to false positive or false negative labels; while still maintaining circa half the number of nick pairs which occur at a frequency above 30. Note that this separation distance is substantially larger than λ-DNA, which is often used as a model system for studying DNA in nanochannels.

The distribution for fractional extension for the subset of nick labels with $L > 30$ μm is shown in Figure 4. The distributions are roughly Gaussian, centered around a mean value equal to the fractional extension in Table II and a standard deviation ≈ 0.05. It is important to note that this standard deviation is not directly related to the variance reported in previous studies[1,16,19,20] as the variance in X/L is not equivalent to the variance in X when the ensemble for X/L contains an underlying distribution in the values of L.[21]

Our motivation for using *E. coli* DNA, rather than human DNA, is that the genome of *E. coli* is relatively GC-even. As a result, we would expect that the effect of % GC content on the persistence length[31] to be attenuated with this organism. However, as indicated in Fig. 5, although the % GC content of the DNA between nick pairs in *E. coli* separated by at least 2,500 bp is peaked near 53% GC, there is still a relatively wide range of % GC content. Fortunately, our restriction to distances $L > 30$ μm substantially tightens the

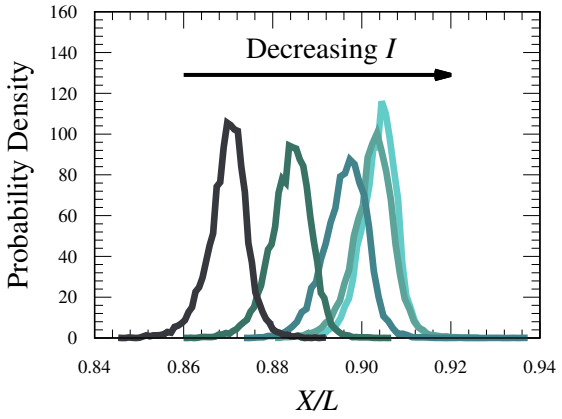

FIG. 4. Probability density of fractional extensions obtained for the five different ionic strengths listed in Table I for nick pairs with $L > 30$ μm.

TABLE II. Details of experimental conditions, amount of data obtained, average fractional extension $\langle X/L \rangle$, and depletion width δ, calculated using the Odijk theory,[3,13] for each ionic strength I. The number of nick pairs refers to those measurements on aligned molecules with separations L that exceed 30 μm. The maximum error in ionic strength is a conservative estimate of the errors due to fluid exchange between experiments. The error for the initial ionic strength is below the number of significant digits. The maximum error in δ is ±2.5 nm owing to the uncertainty in the channel size. Owing to the large separation distances, the error in fractional extension is negligible compared to the uncertainty in the channel size

I (mM)	No. of molecules	Aligned molecules	No. of nick pairs	$\langle X/L \rangle$	δ (nm)
16.9 ± 0.0	12 201	7 839	1 055 121	0.9039	14.8
18.5 ± 1.7	12 195	6 981	899 288	0.9025	14.5
20.0 ± 1.8	12 456	6 490	850 856	0.8963	12.5
44.4 ± 2.0	16 658	10 732	1 539 310	0.8839	10.0
72.2 ± 4.4	11 170	7 249	658 980	0.8698	6.0

distribution. Moreover, Fig. 5 shows that the distribution of these widely separated nick pairs shifts closer to 50% GC, which is approximately equal to the 49.86% GC content of λ-DNA used to parameterize Dobrynin's theory in Eq. (9). Dobrynin's theory has proven to be a good model for λ-DNA in nanoslit confinement,[52] lending confidence to its application

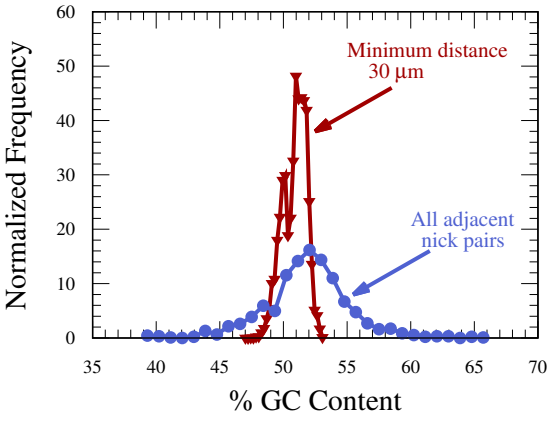

FIG. 5. % GC content for all adjacent nick pairs in the *E. coli* genome separated by at least 2500 bp (•) and those separated by the minimum distance $L = 30$ µm used in our analysis (▼).

here.

The distributions in Figs. 4 and 5 suggest that our choice of *E. coli* DNA and nick pairs separated by $L > 30$ µm is sufficient to exclude contour length and % GC content as contributions to the fractional extension, thus allowing the ionic strength to be the dominant factor affecting the variation in the data.

To convert from the average extension to the depletion length, we use the fractional extension in the Odijk regime[3] with the prefactor for square channels from Burkhardt *et al.*,[13]

$$\left\langle \frac{X}{L} \right\rangle = 1 - 0.18274 \left(\frac{D_{\text{eff}}}{l_{\text{p}}} \right)^{2/3} \tag{12}$$

Inverting this equation, using the persistence length data in Table I, provides D_{eff}. We then compute the depletion length via Eq. (1), noting that the maximum error in δ is dominated by the error in the channel size D.

The resulting values of the depletion length are reported in Table II and are plotted in Figure 6. As we have probed thousands of molecules for each ionic strength, the statistical error in δ is negligible. Figure 6 compares the three models for δ outlined in Section II with the experimental values. It is remarkable that even though the approximation $\delta = w$ is conceptually incorrect, it provides the best agreement with the experimental data. The models for δ in Eqs. (6) and (7) capture the qualitative trend in depletion length with ionic strength but quantitatively differ from the experimental values.

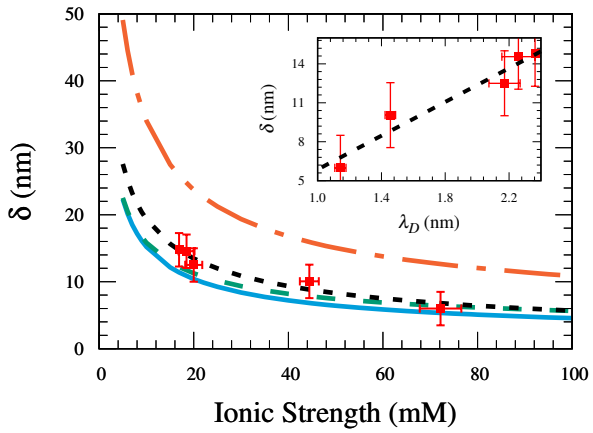

FIG. 6. Depletion length as a function of ionic strength from experiments (red squares), semiflexible chain model (Eq. (6), solid blue line), rod-like model (Eq. (7), dash-dotted orange line), and the approximation $\delta = w$ (dashed green line). The dashed black line is Eq. (13). The inset shows the experimental data and Eq. (13) as a function of the Debye length. The error bars correspond to maximum errors.

The inset of Fig. 6 shows that, as we anticipated in the discussion of the models for the depletion length, the depletion length at these high ionic strengths is proportional to the Debye length. Linear regression to the experimental data reveals that

$$\delta = 6.5\lambda_{\mathrm{D}} - 0.64 \tag{13}$$

with an R^2 value of 0.94. We tested the statistical significance of the intercept term using a hypothesis test with a zero intercept as the null hypothesis. Using the standard error of the intercept and calculating over $n-2$ degrees of freedom, we obtained a p-value of 0.76 for the hypothesis test. This implies that the intercept is not statistically significant and the scaling for δ is essentially of the form we anticipated.

V. DISCUSSION

Equation (13) is the key result of our work. It represents a simple, yet accurate, model for computing the depletion length for ionic strengths where the electrostatic screening length is small. Indeed, inspection of Table I indicates that the Debye length is smaller than any length scale in the problem, and it is substantially smaller than either the DNA persistence

length or the size of the channel. Such strong screening is the best system for using data obtained using a polyelectrolyte like DNA to theories developed for a neutral polymer, so experiments at these ionic strengths[1,16,18,21,40–43] are crucial for comparing theory and experiment.[15]

An outstanding question in the literature is whether the uncertainty in δ in previous comparisons between theory and experiment was a major source of discrepancy. To answer this question, we revisited a trio of previous experiments[18,20,22] that aimed to study the confinement of DNA in the so-called extended de Gennes regime.[5] Strictly speaking, the marginal solution behavior exhibited in the extended de Gennes regime is expected to be valid for channel sizes $l_p \ll D_{eff} \ll l_p^2/w$.[4] While it is infeasible to achieve these strong inequalities using DNA,[15] these experiments[18,20,22] all exhibited a variance in the chain extension that was independent of the channel size. The latter is a key prediction of the extended de Gennes regime,[5,7,8,14] and thus these experiments seem to be a promising data set for testing the theory.

A particularly attractive aspect of the extended de Gennes regime, aside from the relative ease of fabricating nanochannels in this size range, is that there exists an exact theory for the chain extension. Using a mapping between the polymer problem and a one-dimensional weakly self avoiding random walk,[57] Werner and Mehlig showed that the fractional extension of the extended de Gennes regime should be[14]

$$\left\langle \frac{X}{L} \right\rangle = 1.17662 \left(\frac{D_{eff}^2}{l_p w} \right)^{-1/3} \tag{14}$$

Previous work[18,20,22] compared experiment to the theory in Eq. (14) using $\delta = w$ to compute D_{eff}, and all of these experimental analyses noted this approximation as a source of potential systematic error. However, given that we would expect $\delta/D \ll 1$ and the relatively good agreement between the experimental data and $\delta = w$ in Fig. 6, it is not obvious *a priori* that a better model for the depletion length would lead to much change in the residual between the experimentally-measured value of $\langle X/L \rangle$ and that predicted by Eq. (14).

To determine whether our new model indeed corrects for the systematic error using $\delta = w$, we simply calculated D_{eff} for each channel size and ionic strength in the experiments[18,20,22] using Eq. (1) and (13). The residual for a given data point is then defined as the absolute value of the difference between theory and experiment. Figure 7 indicates that the agreement

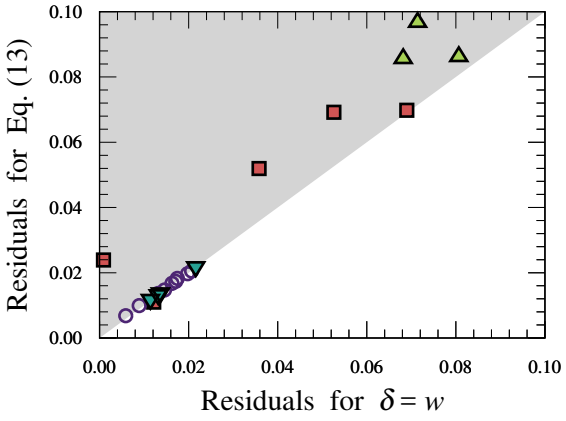

FIG. 7. The residual between the experimentally measured fractional extension and Eq. (14) for the experiments in Ref. 22 (I = 28 mM, ■), Ref. 20 (I = 7.2 mM, ○), and Ref. 18 for l_p/w = 3.0 (I = 3.8 mM, ▲) and l_p/w = 5.8 (I = 78.4 mM, ▼). The residuals are largely unchanged for most of the experiments while points in the shaded region represent data with reduced agreement with theory after correcting for δ.

between theory and experiment is largely unchanged, and in many cases decreased, when using the linear model in Eq. (13) for δ. Overall, the Root Mean Square Error (RMSE) for the measured fractional extension relative to Eq. (14) is 4.9% using our linear model for δ versus 4.1% for $\delta = w$.

The qualitative behavior in Fig. 7 could be anticipated directly from Fig. 6. Theory generally overpredicts the values of fractional extension observed in experiments[14,22] for a given $D_{\text{eff}}^2/l_{\text{p}}w$. Figure 6 shows that values of δ calculated using Eq. (13) are larger than w (Fig. 6), thus decreasing D_{eff} and increasing the deviation from the theoretical prediction. While the ambiguity in D_{eff} was a source of uncontrolled systematic error in these previous studies,[18,20,22] our analysis here shows that it was a minor error and certainly not sufficient to bring theory and experiment into quantitative agreement.

It is not obvious how to reconcile Eq. (13) with theories for the depletion length. Remarkably, over the range of ionic strengths of interest to us, the approximation $\delta = w$ provides the closest agreement with the experimental data amongst the three models in the literature. This helps to rationalize its widespread use, even though this model is fundamentally flawed on both geometrical and chemical grounds. With respect to the other two models, it

is satisfying to see that the experimental data agree with the prediction of a linear dependence $\delta \sim \lambda_D$ for both the rod-like and semiflexible models in the high ionic strength limit. However, their prefactors differ substantially from Eq. (13). One simple reconciliation is that approximations within the models, for example the scaling arguments underlying the semiflexible chain model, are the source of the discrepancy. The prefactors for the scaling arguments would need to be relatively large, however, since the circa two-fold differences between the proportionality constants for these theories and Eq. (13) correspond to e^2 corrections to the F terms in Eq. (8). It also seems unlikely that the increased ionic strength caused by the DNA itself, as suggested by Stein for confinement in blob-like regimes,[27] would improve the result here. In the Odijk regime, the chain is stretched along the channel without backfolding. As a result, we would not expect that distal segments of the DNA would contribute to the local ionic environment.

The best approach to distinguishing between the merits of the rod-like and the semiflexible chain models for the depletion length would be working at even lower ionic strengths, as the logarithmic terms that capture the differences between the models become increasingly important as ionic strength decreases. There is a body of experimental work at low ionic strength[16,52,58–65] that exploits the increased electrostatic repulsion between the DNA and the walls to approach complete extension.[61] Unfortunately, it is challenging to use our approach at such low ionic strengths. Once the double-layer begins to occupy a substantial fraction of the channel size, the mapping between a polyelectrolyte and equivalent neutral chain becomes specious.[66]

VI. CONCLUSION

We have used a massively parallel experimental system to arrive at a relatively simple linear model in Eq. (13) for the depletion length between DNA and a silica surface for ionic strengths in excess of 16.9 mM. From a practical standpoint, Eq. (13) is quite convenient because it can be evaluated without the need to first compute the effective charge density of the DNA. As our model is largely empirical, one should take caution when applying it outside the range of ionic strengths used here. Indeed, although our results suggest that there are some shortcomings in the existing theories for the depletion length in Eqs. (6) and (7), Fig. 2 indicates that the linear relationship between the depletion length and the

Debye length should set in for ionic strengths higher than approximately 5 mM. We view this as a minor shortcoming in our model, as the strategy of mapping from a polyelectrolyte to an equivalent neutral polymer model becomes specious when the Debye length occupies a substantial fraction of either the channel size at lower ionic strengths. This problem is isomorphic to that encountered when applying Stigter's effective width theory[25] at low ionic strengths, since that theory is only valid for interactions in the far field where a Debye-Hückel approximation is reasonable.

We anticipate that this model will find use in the comparison between theories for DNA extension in a nanochannel and in experiments, as the electrostatic screening provided at these ionic strengths is ideally suited for using DNA, a polyelectrolyte, as a model system for examining theories for confining a neutral semiflexible chain in a channel. Figure 7 provides a degree of closure to the question of whether systematic error introduced in experimental analyses by using an incorrect value of δ is the dominant factor causing deviations observed between experiment and theory; the deviations are increased by approximately 20% after correcting for δ. This motivates further investigation into other sources of systematic error in experimental studies and their mapping to theory. The effects of YOYO-1 on the mechanical properties of DNA are only slowly coming into view.[53–55] A correction for the contour length is typically made in experiments with high dye loading, but the persistence length and effective width are considered to be unaffected in the analysis.[22] Several experiments[53,67–71] have reported conflicting results about the effect of dye loading on the persistence length of DNA, while the effect on the DNA effective width has not yet been studied. Finally, theories for DNA extension are often derived explicitly for square nanochannels[14,15] which is not the case for the vast majority of experimental studies. Modifications to existing theories to accommodate rectangular channels[11] may also prove to be an avenue for improving the agreement between experiment and theory.

ACKNOWLEDGMENTS

This work was supported by the National Institutes of Health (NIH R01-HG006851). Computational resources were provided in part by the Minnesota Supercomputing Institute. J.G.R. and H.C. are employees of BioNano Genomics, which is commercializing nanochannel genome mapping.

REFERENCES

[1]W. Reisner, K. J. Morton, R. Riehn, Y. M. Wang, Z. Yu, M. Rosen, J. C. Sturm, S. Y. Chou, E. Frey, and R. H. Austin, "Statics and dynamics of single DNA molecules confined in nanochannels," Phys. Rev. Lett. **94**, 196101 (2005).

[2]M. Daoud and P. G. de Gennes, "Statistics of macromolecular solutions trapped in small pores," J. Phys. **38**, 85–93 (1977).

[3]T. Odijk, "The statistics and dynamics of confined or entangled stiff polymers," Macromolecules **16**, 1340–1344 (1983).

[4]T. Odijk, "Scaling theory of DNA confined in nanochannels and nanoslits," Phys. Rev. E **77**, 060901 (2008).

[5]Y. Wang, D. R. Tree, and K. D. Dorfman, "Simulation of DNA extension in nanochannels," Macromolecules **44**, 6594–6604 (2011).

[6]A. Muralidhar, D. R. Tree, Y. Wang, and K. D. Dorfman, "Interplay between chain stiffness and excluded volume of semiflexible polymers confined in nanochannels," J. Chem. Phys. **140**, 084905 (2014).

[7]L. Dai and P. S. Doyle, "Comparisons of a polymer in confinement versus applied force," Macromolecules **46**, 6336–6344 (2013).

[8]L. Dai, J. R. C. van der Maarel, and P. S. Doyle, "Extended de Gennes regime of DNA confined in a nanochannel," Macromolecules **47**, 2445–2450 (2014).

[9]A. Muralidhar, D. R. Tree, and K. D. Dorfman, "Backfolding of wormlike chains confined in nanochannels," Macromolecules **47**, 8446–8458 (2014).

[10]A. Muralidhar and K. D. Dorfman, "Backfolding of DNA confined in nanotubes: Flory theory versus the two-state cooperativity model," Macromolecules **49**, 1120–1126 (2016).

[11]A. Muralidhar, M. J. Quevillon, and K. D. Dorfman, "The backfolded Odijk regime for wormlike chains confined in rectangular nanochannels," Polymers **8**, 79 (2016).

[12]Y. Yang, T. W. Burkhardt, and G. Gompper, "Free energy and extension of a semiflexible polymer in cylindrical confining geometries," Phys. Rev. E **76**, 011804 (2007).

[13]T. W. Burkhardt, Y. Yang, and G. Gompper, "Fluctuations of a long, semiflexible polymer in a narrow channel," Phys. Rev. E **82**, 041801 (2010).

[14]E. Werner and B. Mehlig, "Confined polymers in the extended de Gennes regime," Phys. Rev. E **90**, 062602 (2014).

[15]E. Werner, G. K. Cheong, D. Gupta, K. D. Dorfman, and B. Mehlig, "One-parameter scaling theory for DNA extension in a nanochannel," Phys. Rev. Lett. **119**, 268102 (2017).

[16]W. Reisner, J. P. Beech, N. B. Larsen, H. Flyvbjerg, A. Kristensen, and J. O. Tegenfeldt, "Nanoconfinement-enhanced conformational response of single DNA molecules to changes in ionic environment," Phys. Rev. Lett. **99**, 058302 (2007).

[17]F. Persson, P. Utko, W. Reisner, N. B. Larsen, and A. Kristensen, "Confinement spectroscopy: Probing single DNA molecules with tapered nanochannels," Nano Lett. **9**, 1382–1385 (2009).

[18]V. Iarko, E. Werner, L. Nyberg, V. Müller, J. Fritzsche, T. Ambjörnsson, J. Beech, J. Tegenfeldt, K. Mehlig, F. Westerlund, and B. Mehlig, "Extension of nanoconfined DNA: Quantitative comparison between experiment and theory," Phys. Rev. E **92**, 062701 (2015).

[19]D. Gupta, J. Sheats, A. Muralidhar, J. J. Miller, D. E. Huang, S. Mahshid, K. D. Dorfman, and W. Reisner, "Mixed confinement regimes during equilibrium confinement spectroscopy of DNA," J. Chem. Phys. **140**, 214901 (2014).

[20]D. Gupta, J. J. Miller, A. Muralidhar, S. Mahshid, W. Reisner, and K. D. Dorfman, "Experimental evidence of weak excluded volume effects for nanochannel confined DNA," ACS Macro Lett. **4**, 759–763 (2015).

[21]W. F. Reinhart, J. G. Reifenberger, D. Gupta, A. Muralidhar, J. Sheats, H. Cao, and K. D. Dorfman, "Distribution of distances between DNA barcode labels in nanochannels close to the persistence length," J. Chem. Phys. **142**, 064902 (2015).

[22]D. Gupta, A. B. Bhandari, and K. D. Dorfman, "Evaluation of blob theory for the diffusion of DNA in nanochannels," Macromolecules **51**, 1748–1755 (2018).

[23]E. T. Lam, A. Hastie, C. Lin, D. Ehrlich, S. K. Das, M. D. Austin, P. Deshpande, H. Cao, N. Nagarajan, M. Xiao, and P.-Y. Kwok, "Genome mapping on nanochannel arrays for structural variation analysis and sequence assembly," Nat. Biotechnol. **30**, 771 (2012).

[24]A. V. Dobrynin, "Electrostatic persistence length of semiflexible and flexible polyelectrolytes," Macromolecules **38**, 9304–9314 (2005).

[25]D. Stigter, "Interactions of highly charged colloidal cylinders with applications to double-stranded DNA," Biopolymers **16**, 1435–1448 (1977).

[26]D. R. Tree, A. Muralidhar, P. S. Doyle, and K. D. Dorfman, "Is DNA a good model polymer?" Macromolecules **46**, 8369–8382 (2013).

[27]W. Reisner, J. N. Pedersen, and R. H. Austin, "DNA confinement in nanochannels: physics and biological applications," Rep. Prog. Phys. **75**, 106601 (2012).

[28]J. Sheats, J. G. Reifenberger, H. Cao, and K. D. Dorfman, "Measurements of DNA barcode label separations in nanochannels from time-series data," Biomicrofluidics **9**, 064119 (2015).

[29]J. G. Reifenberger, K. D. Dorfman, and H. Cao, "Topological events in single molecules of E. coli DNA confined in nanochannels," Analyst **140**, 4887–4894 (2015).

[30]A. Jain, J. Sheats, J. G. Reifenberger, H. Cao, and K. D. Dorfman, "Modeling the relaxation of internal DNA segments during genome mapping in nanochannels," Biomicrofluidics **10**, 054117 (2016).

[31]H.-M. Chuang, J. G. Reifenberger, H. Cao, and K. D. Dorfman, "Sequence-dependent persistence length of long DNA," Phys. Rev. Lett. **119**, 227802 (2017).

[32]J. G. Reifenberger, H. Cao, and K. D. Dorfman, "Odijk excluded volume interactions during the unfolding of DNA confined in a nanochannel," Macromolecules **51**, 1172–1180 (2018).

[33]R. H. Doremus, "Diffusion of water in silica glass," J. Mater. Res. **10**, 2379–2389 (1995).

[34]G. A. Parks, "The isoelectric points of solid oxides, solid hydroxides, and aqueous hydroxo complex systems," Chem. Rev. **65**, 177–198 (1965).

[35]H. Chang, F. Kosari, G. Andreadakis, M. Alam, G. Vasmatzis, and R. Bashir, "DNA-mediated fluctuations in ionic current through silicon oxide nanopore channels," Nano Lett. **4**, 1551–1556 (2004).

[36]D. Stigter, "The charged colloidal cylinder with a Gouy double layer," J. Colloid Interface Sci. **53**, 296–306 (1975).

[37]S. H. Behrens and D. G. Grier, "The charge of glass and silica surfaces," J. Chem. Phys. **115**, 6716–6721 (2001).

[38]R. K. Iler, "The chemistry of silica. 1979," Ed. J. Wiley and Sons, New York (1979).

[39]T. Hiemstra, J. De Wit, and W. Van Riemsdijk, "Multisite proton adsorption at the soil/solution interface of (Hydr) oxides: a new approach. II: Application to various important (Hydr) oxides," J. Colloid Interface Sci. **133**, 105–117 (1989).

[40]L. H. Thamdrup, A. Klukowska, and A. Kristensen, "Stretching DNA in polymer nanochannels fabricated by thermal imprint in PMMA." Nanotechnology **19**, 125301 (2008).

[41]P. Utko, F. Persson, A. Kristensen, and N. B. Larsen, "Injection molded nanofluidic chips: Fabrication method and functional tests using single-molecule DNA experiments," Lab Chip **11**, 303–308 (2011).

[42]E. Werner, F. Persson, F. Westerlund, J. O. Tegenfeldt, and B. Mehlig, "Orientational correlations in confined DNA," Phys. Rev. E **86**, 041802 (2012).

[43]M. Alizadehheidari, E. Werner, C. Noble, M. Reiter-Schad, L. K. Nyberg, J. Fritzsche, B. Mehlig, J. O. Tegenfeldt, T. Ambjörnsson, F. Persson, and F. Westerlund, "Nanoconfined circular and linear DNA: Equilibrium conformations and unfolding kinetics," Macromolecules **48**, 871–878 (2015).

[44]A. R. Hastie, L. Dong, A. Smith, J. Finklestein, E. T. Lam, N. Huo, H. Cao, P.-Y. Kwok, K. R. Deal, J. Dvorak, M.-C. Luo, Y. Gu, and M. Xiao, "Rapid genome mapping in nanochannel arrays for highly complete and accurate de novo sequence assembly of the complex Aegilops Tauschii genome," PLoS One **8**, e55864 (2013).

[45]A. C. Y. Mak, Y. Y. Y. Lai, E. T. Lam, T.-P. Kwok, A. K. Y. Leung, A. Poon, Y. Mostovoy, A. R. Hastie, W. Stedman, T. Anantharaman, W. Andrews, X. Zhou, A. W. C. Pang, H. Dai, C. Chu, C. Lin, J. J. K. Wu, C. M. L. Li, J.-W. Li, A. K. Y. Yim, S. Chan, J. Sibert, Ž. Džakula, H. Cao, S.-M. Yiu, T.-F. Chan, K. Y. Yip, M. Xiao, and P.-Y. Kwok, "Genome-wide structural variation detection by genome mapping on nanochannel arrays," Genetics **202**, 351–362 (2016).

[46]S. K. Das, M. D. Austin, M. C. Akana, P. Deshpande, H. Cao, and M. Xiao, "Single molecule linear analysis of DNA in nano-channel labeled with sequence specific fluorescent probes," Nucleic Acids Res. **38**, e177–e177 (2010).

[47]T. Su, S. K. Das, M. Xiao, and P. K. Purohit, "Transition between two regimes describing internal fluctuation of DNA in a nanochannel," PLoS One **6**, e16890 (2011).

[48]A. Valouev, *Shotgun optical mapping: a comprehensive statistical and computational analysis* (University of Southern California, 2006).

[49]U. Dobrindt, F. Agerer, K. Michaelis, A. Janka, C. Buchrieser, M. Samuelson, C. Svanborg, G. Gottschalk, H. Karch, and J. Hacker, "Analysis of genome plasticity in pathogenic and commensal Escherichia coli isolates by use of DNA arrays," J. Bacteriol. **185**, 1831–1840 (2003).

[50]T. M. Conrad, A. R. Joyce, M. K. Applebee, C. L. Barrett, B. Xie, Y. Gao, and B. Ø. Palsson, "Whole-genome resequencing of Escherichia coli K-12 MG1655 undergoing short-

term laboratory evolution in lactate minimal media reveals flexible selection of adaptive mutations," Genome Biol. **10**, R118 (2009).

[51]P. L. Freddolino, S. Amini, and S. Tavazoie, "Newly identified genetic variations in common Escherichia coli MG1655 stock cultures," J. Bacteriol. **194**, 303–306 (2012).

[52]C.-C. Hsieh, A. Balducci, and P. S. Doyle, "Ionic effects on the equilibrium dynamics of DNA confined in nanoslits," Nano Lett. **8**, 1683–1688 (2008).

[53]B. Kundukad, J. Yan, and P. S. Doyle, "Effect of YOYO-1 on the mechanical properties of DNA," Soft Matter **10**, 9721–9728 (2014).

[54]K. Günther, M. Mertig, and R. Seidel, "Mechanical and structural properties of YOYO-1 complexed DNA," Nucleic Acids Res. **38**, 6526–6532 (2010).

[55]K. D. Dorfman, "The statistical segment length of DNA: Opportunities for biomechanical modeling in polymer physics and next-generation genomics," J. Biomech. Eng. **140**, 020801 (2018).

[56]Y. Wang, W. F. Reinhart, D. R. Tree, and K. D. Dorfman, "Resolution limit for DNA barcodes in the Odijk regime," Biomicrofluidics **6**, 014101 (2012).

[57]R. Van der Hofstad, F. Den Hollander, and W. König, "Weak interaction limits for one-dimensional random polymers," Probab. Theory and Relat. Fields **125**, 483–521 (2003).

[58]K. Jo, D. M. Dhingra, T. Odijk, J. J. de Pablo, M. D. Graham, R. Runnheim, D. Forrest, and D. C. Schwartz, "A single-molecule barcoding system using nanoslits for DNA analysis," Proc. Natl. Acad. Sci. USA **104**, 2673–2678 (2007).

[59]C. Zhang, F. Zhang, J. A. van Kan, and J. R. C. van der Maarel, "Effects of electrostatic screening on the conformation of single DNA molecules confined in a nanochannel," J. Chem. Phys. **128**, 06B611 (2008).

[60]D. J. Bonthuis, C. Meyer, D. Stein, and C. Dekker, "Conformation and dynamics of DNA confined in slitlike nanofluidic channels," Phys. Rev. Lett. **101**, 108303 (2008).

[61]Y. Kim, K. S. Kim, K. L. Kounovsky, R. Chang, G. Y. Jung, J. J. de Pablo, K. Jo, and D. C. Schwartz, "Nanochannel confinement: DNA stretch approaching full contour length," Lab Chip **11**, 1721–1729 (2011).

[62]P.-k. Lin, C.-C. Hsieh, Y.-L. Chen, and C.-F. Chou, "Effects of topology and ionic strength on double-stranded DNA confined in nanoslits," Macromolecules **45**, 2920–2927 (2012).

[63]K. L. Kounovsky-Shafer, J. P. Hernández-Ortiz, K. Jo, T. Odijk, J. J. De Pablo, and D. C. Schwartz, "Presentation of large DNA molecules for analysis as nanoconfined dumbbells,"

Macromolecules **46**, 8356–8368 (2013).

[64]J. Lee, S. Kim, H. Jeong, G. Y. Jung, R. Chang, Y.-L. Chen, and K. Jo, "Nanoslit confined DNA at low ionic strengths," ACS Macro Lett. **3**, 926–930 (2014).

[65]K. L. Kounovsky-Shafer, J. P. Hernandez-Ortiz, K. Potamousis, G. Tsvid, M. Place, P. Ravindran, K. Jo, S. Zhou, T. Odijk, J. J. de Pablo, and D. C. Schwartz, "Electrostatic confinement and manipulation of DNA molecules for genome analysis," Proc. Natl. Acad. Sci. USA **114**, 13400–13405 (2017).

[66]G. K. Cheong, X. Li, and K. D. Dorfman, "Wall depletion length of a channel-confined polymer," Phys. Rev. E **95**, 022501 (2017).

[67]S. R. Quake, H. Babcock, and S. Chu, "The dynamics of partially extended single molecules of DNA," Nature **388**, 151 (1997).

[68]T. Berge, N. S. Jenkins, R. B. Hopkirk, M. J. Waring, J. M. Edwardson, and R. M. Henderson, "Structural perturbations in DNA caused by bis-intercalation of ditercalinium visualised by atomic force microscopy," Nucleic Acids Res. **30**, 2980–2986 (2002).

[69]A. Sischka, K. Toensing, R. Eckel, S. D. Wilking, N. Sewald, R. Ros, and D. Anselmetti, "Molecular mechanisms and kinetics between DNA and DNA binding ligands," Biophys. J. **88**, 404–411 (2005).

[70]M. Maaloum, P. Muller, and S. Harlepp, "DNA-intercalator interactions: structural and physical analysis using atomic force microscopy in solution," Soft Matter **9**, 11233–11240 (2013).

[71]N. Shi and V. M. Ugaz, "An entropic force microscope enables nano-scale conformational probing of biomolecules," Small **10**, 2553–2557 (2014).